EVOLUTIONARY BENEFITS OF LATENCY IN WITHIN-HOST HIV INFECTION DYNAMICS

A Dissertation
Presented to
The Academic Faculty

By

Qi An

In Partial Fulfillment
of the Requirements for the Degree
Master of Science in the
School of Biological Sciences

Georgia Institute of Technology

May 2019

EVOLUTIONARY BENEFITS OF LATENCY IN WITHIN-HOST HIV INFECTION DYNAMICS

Approved by:

Dr. Joshua S. Weitz
School of Biological Sciences
School of Physics
Georgia Institute of Technology

Dr. Samuel P. Brown
School of Biological Sciences
Georgia Institute of Technology

Dr. Daniel Coombs
Department of Mathematics
University of British Columbia

Date Approved: April 17, 2019

ACKNOWLEDGEMENTS

I would like to thank my advisor, Dr. Joshua Weitz for guidance and support throughout this year. From the perspective of academics, Joshua not only provided me with comprehensive systematic training in quantitative biology but also trained me to think scientifically and become an independent researcher. The way I think about a project and organize a paper is much influenced by his guidance.

I would like to thank Guanlin Li and Dr. Michael Cortez. Together with Dr. Weitz, they firstly derived the equations to implement Levin's loop analysis method in the viral dynamics modeling research, which become the basis of this thesis.

I would also like to thank Dr. Daniel Coombs and Dr. Sam Brown for serving as thesis committee members and providing direct guidance on this work. They contributed to the framework of my model.

I would like to thank those directly involved as mentors throughout my graduate life. Dr. Mark Borodovsky and Dr. Jeffrey Skolnick provided me with the rotation experience and trained me on network analysis and bioinformatics algorithm development.

I would also like to thank the Bioinformatics Graduate Program for funding and administrative support. Dr. King Jordan, Ms. Lisa Redding, and Ms. Kim Chung provided very effective information and assistance to my graduation.

I would like to thank all of the members of the Weitz group for their help, especially Yu-Hui Lin for providing suggestions on both the research project and career development. I also want to thank Ashley Coenen for help in English writing.

Finally, I want to thank my family. The last semester of graduate life is chaotic and highly stressful with pressure from research and uncertainty in the future. Despite a 12-hour time difference, my parents provided unconditional mental and financial support to help me survive this period. My sister, as a junior high school student, always talks about my research project with the highest curiosity and provides perspectives outside science.

TABLE OF CONTENTS

LIST OF TABLES

LIST OF FIGURES

SUMMARY

HIV is a retrovirus that infects helper T cells (CD4 + T cells) in the human immune system. At the cellular scale, HIV generates both actively and latently infected cells. Actively infected cells produce mature virions and are often the primary target of antiretroviral therapies. In contrast, latently infected T cells can do not produce virus particles, are hard to detect and treat, and can be reactivated to produce new virions. Understanding the dynamics of latent infections is critical to the development of strategies to treat and control the spread of HIV.

In this thesis, we study a variant of within-host models of HIV infection dynamics including proliferation of both susceptible and latently infected CD4+ cells. In this model, HIV infection of susceptible cells can result in acute or latent infections. The key innovation here is to identify the relative contributions of the active and latent pathways towards viral fitness, both in the initial and later stages of the within-host dynamics. We do so by leveraging a new approach to decomposing viral fitness developed in the context of phage-bacteria interactions. Our work highlights how variation in susceptible cell densities, viral life history traits, and retroviral therapies jointly influence dynamic selection pressures for active and latent infections.

CHAPTER 1
INTRODUCTION AND BACKGROUND

Human Immunodeficiency Virus (HIV) is a virus that infects humans by attacking helper T cells (CD4 + T cells) in the immune system. During infection, HIV proliferates by manipulating genetic mechanisms to make copies of the viral genome. Infected CD4 cells will die in large numbers, leading to loss of immune system function and increasing the risk of opportunistic infections[1, 2, 3].

As a retrovirus, the life cycle of HIV is mainly composed of three steps: 1) Fusion of virus and host membrane and injection of virus genome into host cell; 2) Insertion of virus genome into the host genome and replicate; 3) Production of envelope proteins and the assembly of new free virions[4, 5]. Therefore, HIV infection dynamics can be divided into two categories at the cellular scale: acute infection and latent infection. In an acute infection, virus replicates in large quantities and produces new virus particles with an elevated clearance rate of the infected cell[6]. In the latent infection, virus genomes are in a resting state. They replicate with the host genome without assembly of new virions. Latently infected cells can persist within the patient for decades and can reactivate to become acutely infected cells.

Antiretroviral therapy (ART) is a clinically recommended HIV treatment regimen[7]. ART controls infection by blocking protein binding reactions in the life cycle of HIV. ART eliminates most acutely infected cells, inhibits viral replication, protects the function of the immune system, and reduces viral load to undetectable values. Hence, ART prevents HIV infected patients from deteriorating to AIDS. However, ART cannot clear latent cells. Latent cells persist within patients even after decades of ART treatment[8, 9]. After removal of the treatment, the latent cells can be reactivated to produce new viral particles[10, 11, 12]. Many studies have shown that HIV persistence is mainly due to the proliferation

of latent cells[13, 14, 15]. Therefore, understanding the mechanisms of host HIV infection, especially the mechanism of HIV latency, is critical to our strategy to optimize HIV treatment.

There have been many studies on the use of theoretical ecology and computational biology methods for human HIV infection, some of which focus on latent cells[13, 14, 15, 16, 17]. However, quantitative studies of latent cell proliferation and their contribution to infection are still rare. In this thesis, we constructed a deterministic model of host HIV infection dynamics based on modifications to the classical HIV viral infection model.

Based on the model, we simulated and analyzed the virus-free, initial infection and late infection. We use an innovation - loop analysis - to show that the infectivity of a virus can be expressed as the combination of different infection paths. We addressed the effects of latency and reactivation rates on cell density and fitness. In doing so, we propose two latent infection strategies: constant and adaptive. We analyzed and compared the two strategies separately emphasized on the latent cell density.

CHAPTER 2

METHODS

2.1 General modeling framework

We develop a deterministic model for with-in host HIV infection. We model the dynamics between five players, susceptible CD4+ T cells (T), exposed cells (E), acutely infected cells (I), latently infected cells (L) and virus (V). Each of the variables denotes the cell density or viral load (cells/ml). We assume the system is well-mixed and not spatial based. At any location in the system, cells have the same concentration and the same probability of interaction with other players.

In this system, susceptible T cells are generated from thymus and enter the system with a constant rate λ. Free virus particles infect susceptible T cells and generate an exposed cell at the rate proportional to the product of T cell density and viral load, βVT. Exposed cells become infected with a rate μ, and choose to be latently infected with probability p and acutely infected with probability $1 - p$. Latent cells can reactivate to become acutely infected cells with a constant rate η. Free virus particles bud from acutely infected cells at rate k for new infections. All states of cells and virus decay with a constant rate. Notably, both T cells and latent cells (L) grow linearly with the rate of b_0 and b_0', respectively. Figure 1 shows a schematic description of this model.

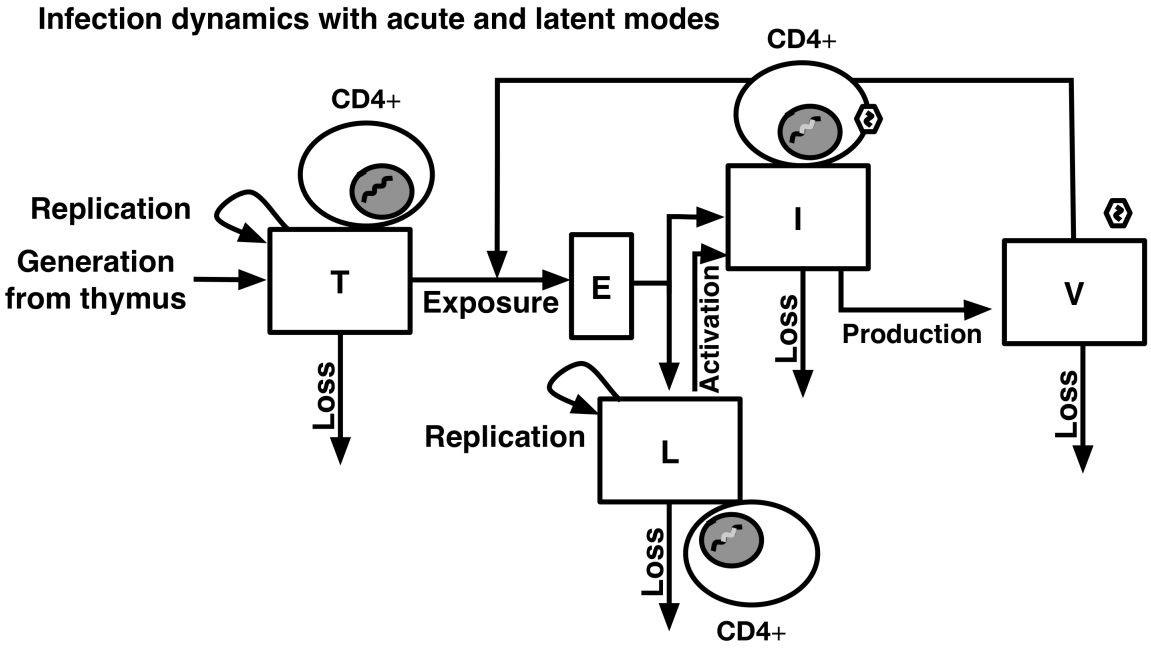

Figure 2.1: A population dynamics model of the with-in host virus infection with a schematic illustration of reactions and cell types. Grey circles: T cells. White hexagons: virus particles. Black wavy line inside cells: cell genome. White wavy line: virus genome. T state: susceptible CD4+ cells. I state: acutely infected cells, with virus genome inserted into host genome, producing new virus particles. L state: latently infected cells, with virus genome inserted into host genome, not producing new virus particles. Image credit: Joshua S. Weitz.

2.1.1 Deterministic model

Based on the reactions described above, we construct a deterministic model as below:

$$
\begin{aligned}
\dot{T} &= \underbrace{\lambda}_{\text{Influx}} + \underbrace{b_0 T}_{\text{Growth}} - \underbrace{\beta V T}_{\text{Infection}} - dT \\
\dot{E} &= \underbrace{\beta V T}_{\text{Infection}} - \underbrace{\mu E}_{\text{Conversion}} - dE \\
\dot{I} &= \underbrace{(1-p)\mu E}_{\text{Acute infection}} + \underbrace{\eta L}_{\text{Reactivation}} - aI \\
\dot{L} &= \underbrace{p\mu E}_{\text{Latent infection}} + \underbrace{b_0' L}_{\text{Growth}} - \underbrace{\eta L}_{\text{Reactivation}} - d' L \\
\dot{V} &= \underbrace{kI}_{\text{Budding}} - \underbrace{\beta V T}_{\text{Infection}} - mV
\end{aligned}
\tag{2.1}
$$

Here we use ordinary differential equations to describe the time evolution of cell density and viral load level. It's worth noting that in this model, new infection cause a reduction in the virus particles and susceptible cells at the same time. Exposed cells decay at the same rate with the susceptible cells. This model is modified based on the model of Conway and Perelson's work[16].

2.2 Biophysical parameters

Reference value or range for the model parameters are obtained from literature as shown in Table 1. The majority of parameters are taken from Conway and Perelson[16, 18]. Parameters including the probability of choosing latency (p) and reactivation rate (η) are varied slightly around the reference value to study the impact of parameters on the dynamics. The growth rate of latently infected cells (b_0') has no reference values. We set $d' < b_0' < d' + \eta$. With this bound, the growth rate exceeds the death rate and ensures latent cell's growth. However, it will not grow exponentially with reactivation. Therefore, the vertical fitness is greater than 1 without reactivation and less than 1 with reactivation.

Table 2.1: Parameters used in simulation, modified from Conway and Perelson. [16]

Notation	Description	Range	Unit
λ	Influx rate of T cell	10^4	Cells/ml/day
b_0	Growth rate of T	0.005	day^{-1}
b_0'	Reproduction rate of L	0.0045	day^{-1}
d	Decay rate of T and E	0.01	day^{-1}
d'	Decay rate of L	0.004	day^{-1}
a	Decay rate of I	1	day^{-1}
m	Decay rate of free virions	23	day^{-1}
β	Infection rate	1.5×10^{-8}	$ml\ virion^{-1}\ day^{-1}$
μ	Conversion rate	1	day^{-1}
p	Probability of latency	10^{-6}	1
η	Reactivation rate	0.001	day^{-1}
k	Virus production rate	2000	day^{-1}

2.3 Computational analysis and simulation methods

To assess invasibility of HIV at early infection, we use the basic reproduction number of the pathogen (R_0) to measure virus fitness. R_0 is the expected number of new infections caused by a single infected cell during its whole life cycle in an otherwise uninfected environment. When $R_0 > 1$, every infected cell produces more than one newly infected cell and the infection will take off in the system; otherwise, the infection would be eliminated from the system[1].

Here we use the Next Generation Matrix method to calculate R_0. First, we use the Jacobian matrix to linearize our nonlinear ODE system near the pathogen-free equilibrium. Then we decompose the Jacobian matrix into a transmission part (T) describing the generation of new infections and transition part (Σ) describing the transitions in infected states[19, 20, 21, 22]. According to the NGM theory, R_0 could be calculated as the dominant eigenvalue of matrix $K_L = -T\Sigma^{-1}$. The element $K_{L,ij}$ of NGM K_L is the expected number of new infections with the infected state i, generated by one individual in infected state j. See Appendix A for specific calculations in our model.

The biological meaning of R_0 is interpreted with Levin's loop analysis method[23, 24]. We decompose the generation of new infections as separate singular paths and calculate the fitness of each path.

For long term infection, we combine the mathematical analysis with simulation method to observe the evolution of cell density and fitness with time. After simulation for enough time length, we regenerate the virus fitness by calculating the effective reproduction number (see detail discussion in Section 3.3).

Simulation is based on Python 3.7.2, Conda 4.6.11 and package integrate.odeint. All simulation codes and results are available in the Appendix.

CHAPTER 3

RESULTS

3.1 Parasite free steady state analysis

We start by analyzing a parasite free system before infection. In a parasite free environment, T cell is the only player in the system. By setting all other states as 0, the nonlinear system's dynamics can be reduced to a linear equation about T cell density:

$$\dot{T} = \lambda + b_0 T - dT \tag{3.1}$$

Hence, the equilibrium density of T cells before infection could be solved as:

$$T^\star = \frac{\lambda}{d - b_0}, b_0 < d \tag{3.2}$$

Since $b_0 < d$, $T^\star > 0$. It means that the growth rate of susceptible T cells is less than the decay rate. Without constant immigration from the thymus, T cells would die out. This equilibrium density is used for the initial condition in simulation.

3.2 Fitness analysis in early infection

3.2.1 Next Generation Matrix calculation

Consider the initial infection, where a small amount of virus particles are introduced into the susceptible CD4+ T cell group. In this scenario, we assume T cell load stays stable at $T^\star$ is a short time scale. Therefore, the dynamics reduce to a linear system around the pathogen-free equilibrium, $[T^\star, 0, 0, 0, 0]$. Using the next generation matrix method, we calculated the transition, transmission matrix and NGM (See Appendix A for detailed

calculation):

$$K_L = -T\Sigma^{-1} = \begin{bmatrix} \Phi_{E\to E} & \Phi_{I\to E} & \Phi_{L\to E} & \Phi_{V\to E} \\ 0 & 0 & 0 & 0 \\ \Phi_{E\to L} & 0 & \Phi_{L\to L} & 0 \\ 0 & 0 & 0 & 0 \end{bmatrix} \tag{3.3}$$

Since there are four infected states in our system, our NGM matrix $K_L = -T\Sigma^{-1}$ has the size of 4×4. However, this matrix is not full rank since the second and fourth row of K_L are all zeros. In our model, individuals cannot enter the I or V state immediately after infection[21]. Therefore we only need two states, E and L, to determine R_0. Hence, we reduce NGM to a 2×2 matrix to simplify calculation[23]:

$$\Phi = Q^T K_L Q = \begin{bmatrix} \Phi_{E\to E} & \Phi_{L\to E} \\ \Phi_{E\to L} & \Phi_{L\to L} \end{bmatrix}, Q = \begin{bmatrix} 1 & 0 & 0 & 0 \\ 0 & 0 & 1 & 0 \end{bmatrix} \tag{3.4}$$

R_0, as the dominant eigenvalue of matrix Φ, could be calculated as:

$$\begin{aligned} R_0 &= \frac{(\Phi_{E\to E} + \Phi_{L\to L}) \pm \sqrt{(\Phi_{E\to E} - \Phi_{L\to L})^2 + 4\Phi_{L\to E}\Phi_{E\to L}}}{2} \\ \Phi_{E\to E} &= \left(\frac{\mu}{d+\mu}\right)\left(\frac{k}{a}\right)\left(\frac{\beta T^\star}{\beta T^\star + m}\right)\left(\frac{d'(1-p)+\eta}{d'+\eta}\right) \\ \Phi_{L\to E} &= \left(\frac{\beta T^\star}{\beta T^\star + m}\right)\left(\frac{k}{a}\right)\left(\frac{\eta}{d'+\eta}\right) \\ \Phi_{E\to L} &= \left(\frac{b_0'}{d'+\eta}\right)\left(\frac{\mu p}{d+\mu}\right) \\ \Phi_{L\to L} &= \frac{b_0'}{d'+\eta} \end{aligned} \tag{3.5}$$

3.2.2 R_0 in early infection is a combination of three different infection paths

We have mathematically calculated R_0, the biological understanding, however, is not straightforward. Here we use Levin's loop analysis method to interpret R_0 as a combination of

one-generation and two-generation transmission loops. This interpretation is first derived by Guanlin Li et al[23] for temperate phage infection models.

A one-generation loop is defined as a transmission path that starts and ends with the same infected state without revisiting any states. There are three types of one-generation loops in the system: lytic loop, lyso-lytic loop, and latent loop.

The lytic loop: $E \rightarrow I \rightarrow V \rightarrow E$, includes the reactions of conversion to acute infected state, budding of virus and new infections. New infection in a single lytic group is denoted as P_1:

$$P_1 = \underbrace{\left(\frac{\mu}{d+\mu}\right)(1-p)}_{E\rightarrow I}\underbrace{\left(\frac{k}{a}\right)}_{I\rightarrow V}\underbrace{\left(\frac{\beta T^\star}{\beta T^\star + m}\right)}_{V\rightarrow E} \tag{3.6}$$

Here, $\frac{\mu}{d+\mu}$ is the probability of conversion to infected states before decay of E; $(1-p)$ is the probability of choosing acute infection; $\frac{k}{a}$ is budding rate; $\frac{\beta T^\star}{\beta T^\star + m}$is the probability of infecting a new susceptible cell before decay of V.

Similarly, we calculate the new infection caused in lyso-lytic loop ($E \rightarrow L \rightarrow I \rightarrow V \rightarrow E$, including the reactions of conversion to latent infection, reactivate to be acute, budding and new infections) as P_2:

$$P_2 = \underbrace{\left(\frac{\mu}{d+\mu}\right)p}_{E\rightarrow L}\underbrace{\left(\frac{\eta}{d'+\eta}\right)}_{L\rightarrow I}\underbrace{\left(\frac{k}{a}\right)}_{I\rightarrow V}\underbrace{\left(\frac{\beta T^\star}{\beta T^\star + m}\right)}_{V\rightarrow E} \tag{3.7}$$

And the new infection caused in the latent loop ($L \rightarrow L$, including the linear growth of latent cells) as P_3:

$$P_3 = \underbrace{\frac{b_0'}{d'+\eta}}_{L\rightarrow L} \tag{3.8}$$

The reproduction number of the three loops can be easily figured out in R_0: $P_1 + P_2 = \Phi_{E\rightarrow E}, P_3 = \Phi_{L\rightarrow L}$. Both the lytic loop and lyso-lytic loop are horizontal transmissions

(new infection is generated by cell interactions), and the latent loop is vertical transmission (new infection is generated by cell growth). Therefore, we could also denote $\Phi_{E\to E}$ as horizontal reproduction number and $\Phi_{L\to L}$ as vertical reproduction number.

Two-generation loops are concatenations of two one-generation loops. Every single one-generation loop can repeat twice to form a two-generation loop (lytic$\bigoplus$lytic, lyso-lytic$\bigoplus$lyso-lytic, latent$\bigoplus$latent), or concatenate with a different loop that has intersect state (lytic$\bigoplus$lysolytic, lysolytic$\bigoplus$lytic, latent$\bigoplus$lyso-lytic, lyso-lytic$\bigoplus$latent). However the lytic loop and latent loop has no shared states, hence, the two loops are disjoint and cannot concatenate.

With all the loop reproduction numbers above, we can rewrite the R_0 equation as[23]:

$$R_0 = \frac{(P_1 + P_2 + P_3) + \sqrt{P_1^2 + P_2^2 + P_3^2 + 2P_1P_2 + 2P_2P_3 - 2P_1P_3}}{2} \tag{3.9}$$

We could interpret R_0 as the average reproduction number of one-generation loops and two-generation loops. We subtract $2P_1P_3$ from the two-generation loops since the two loops are disjoint. The reproduction number of two-generation loops are discounted by taking square root to de-dimensionalize with the one-generation loops.

3.3 Fitness analysis in long-term infection

3.3.1 Effective reproduction number and post-infection strategies

Consider the scenario where acutely infected cells are the only infected cell state present in the system. After the initial infection, a small number of virions infect new susceptible cells and create new virions for more infection. As a loss, susceptible cells are reduced. When the susceptible cell density decreases so low, the rate of new infection βVT also decreases. Therefore, the probability for a virion to make new infection before decay, $\frac{\beta T}{\beta T+m}$ tends to be zero and cannot generate any new infections. With the presence of latent state cells, however, it is possible for the infected cell to enter latent states and proliferate,

thereby leading to an increase in vertical fitness when susceptible cells are not abundant in the environment.

To quantitatively investigate the evolutionary benefit of latency, we introduce the concept of effective reproduction number. Suppose the environment is locally stable in every short time period, based on our well-mixed system assumption, we could linearize the system's nonlinear dynamics around the current environment $[T, E, I, L, V]$. In this case, the infection dynamics is dependent on the current cell density only. The effective reproduction number is calculated in the same way as the basic reproduction number at the early stage of infection, replacing $T^\star$ (parasite free equilibrium) with the current cell density T.

Here we apply two distinct strategies in long-term virus infections to evaluate the potential feedback between dynamics and viral strategies:

1. Virus choose latency with a constant probability p in the whole dynamics process (referred to as constant strategy in below); 2. Virus choose latency with a locally adaptive probability p to the environment, i.e. choose the probability that maximizes the effective reproduction number at the current time point(referred to as adaptive strategy in below).

We use both calculation and simulation methods to observe the dynamics in long-term infection.

3.3.2 Fitness analysis with constant strategy

The goal in this section is to understand the dynamics of cell density and fitness by calculating the effective reproduction number. We first simulate with the constant strategy. Figure 2.1 shows simulation of cell density dynamics with four different constant latent probabilities: $p = 10^{-4}, 10^{-5}, 10^{-6}, 10^{-7}$. The latent cell dynamics (red line in Figure 3.1) shows high sensitivity to the change of p. After long term simulation, density of the latent cells is proportional to the latent probability. Other states, however, are only slightly impacted by the change of p, since latent cells only take a small proportion in the whole system. Table 3.1 shows the cell density after long-term simulation.

Table 3.1: Cell density after simulation for 10000 days. Infected cells choose latency with constant strategy.

p	T density	E density	I density	L density
10^{-4}	782321.73	11938.02	5969.60	1186.38
10^{-5}	782391.30	11937.34	5968.73	118.63
10^{-6}	782398.25	11937.27	5968.64	11.86
10^{-7}	782398.95	11937.27	5968.63	1.19

We also mathematically calculated the steady states and discovered that $L^\star$ is nearly proportional to p, while $T^\star, E^\star, I^\star, V^\star$ are only related to $(1-p)$. Therefore, varying p between 10^{-4} and 10^{-7} has a slight impact on the other states. See section 3.3.2.4 and Appendix B for detailed calculation and discussion.

Total R_{eff} combines fitness via all three single infection loops

After simulation, we use the simulated cell density to regenerate the dynamics of total effective reproduction number and reproduction number of the lytic loop, lyso-lytic loop and latent loop (P_1, P_2, P_3). Figure 3.2 (Up-left) shows the dynamics of regenerated R_{eff} with constant strategy, $p = 10^{-6}$. Surprisingly, the total R_{eff} appears to be close to the maximal reproduction numbers in three single loops. Even with such a small probability of choosing latency, the total fitness R_{eff} can be close to fitness via latent growth only when horizontal growth decreases quickly.

We could use mathematical calculation to validate this result. P_2 is proportional to p. When p is around 0, $P_2 \sim 0$:

$$\begin{aligned} R_0 &\sim \frac{(P_1+P_3)+\sqrt{(P_1+P_3)^2-4P_1P_3}}{2} \\ &= \frac{(P_1+P_3)+\sqrt{(P_1-P_3)^2}}{2} \\ &= max\{P_1, P_3\} \end{aligned} \tag{3.10}$$

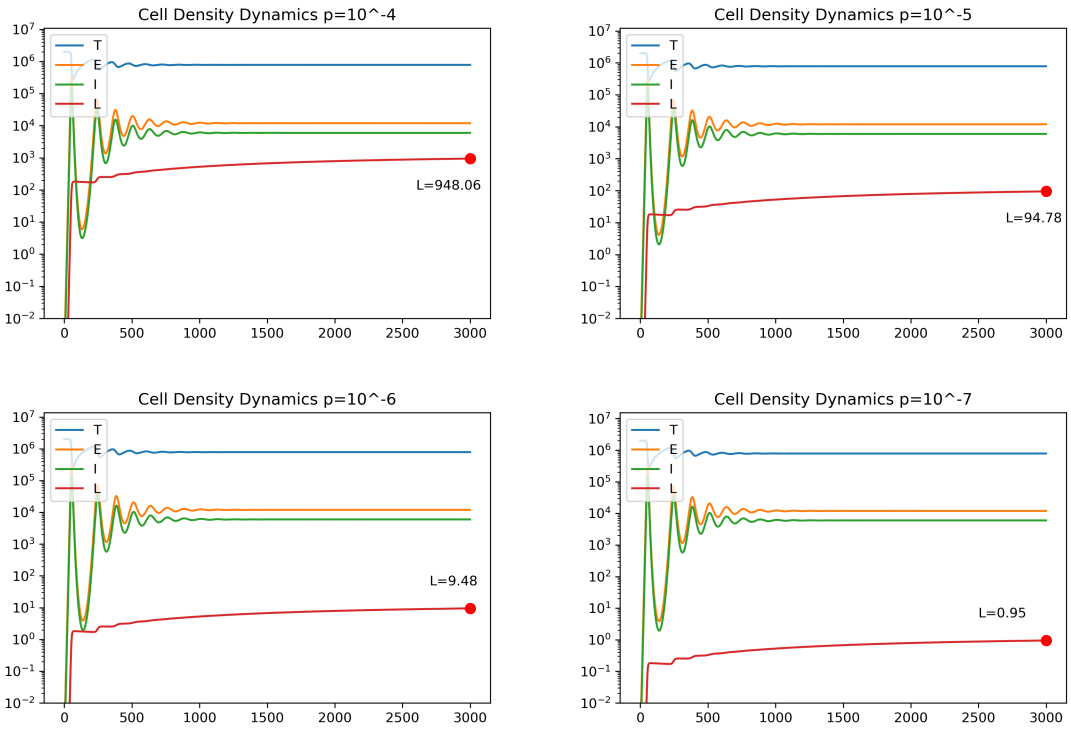

Figure 3.1: Simulation on cell density dynamics with time for 3000 days, $\eta = 10^{-3}$. Infected cells choose latency with constant strategy, $p = 10^{-4}$,10^{-5} ,10^{-6},10^{-7}. Horizontal label: Time (/day). Vertical label: Cell density (Log transformed).

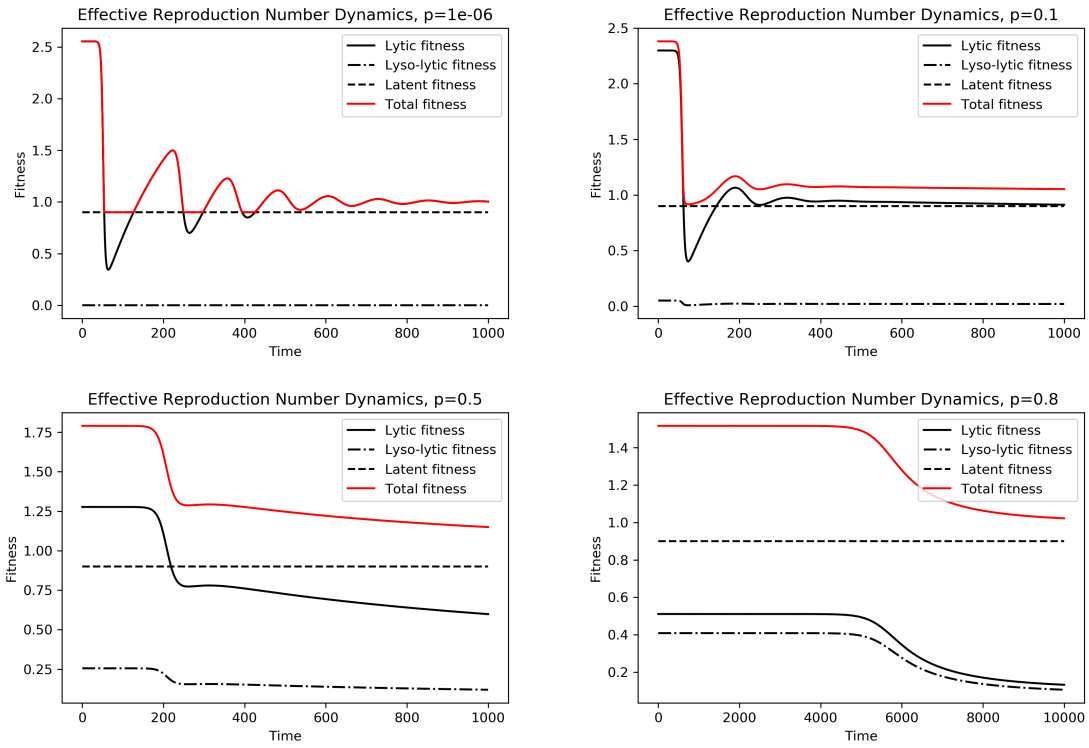

Figure 3.2: Dynamics of regenrated effective reproduction number with simulated cell and virion densities. Red line: Total R_{eff}. Black line: Lytic loop fitness (P_1). Black dot dash line: Lyso-lytic loop fitness (P_2). Black dash line: Latent loop fitness (P_3). Infected cells choose latency with constant strategy, $p = 10^{-6}$ (Up-left),0.1 (Up-right),0.5 (Down-left), 0.8 (Down-right). Horizontal label: Time (/day). Vertical label: Fitness.

Actually, the total fitness is larger than fitness via all three single infection loops, i.e. $R_{\text{eff}} > P_1, R_{\text{eff}} > P_2, R_{\text{eff}} > P_3$. See Appendix B for detailed calculation. Figure 3.2 shows when p gets larger ($p = 0.1, 0.5, 0.8$), reproduction number in every single loop decreases strikingly after long-term infection. The total R_{eff} takes combination of all three loops and still converges to 1.

Sensitivity analysis on R_{eff}

Long-term infection leads to a decrease in susceptible cell density. We are also interested in how the probability of "entering latent state" (latent probability, p) and rate of "leaving latent state" (reactivation rate, η) affects the viral fitness. Therefore, parameter sensitivity analysis of R_{eff} are performed on T, η, p.

We first analyze the sensitivity of T and η with a fixed latent probability p around the point $T = T^\star, \eta = 10^{-3}$. Figure 3.3 shows the contour platte of R_{eff} value. Here we vary T between $0.1 \sim 1.5 \times T^\star$ and vary η between $0 \sim 0.01$, both are linearly stepped. It shows that when p is small, η has slight impact on R_{eff} compare to T; when p gets larger, η starts to affect the fitness. It corresponds to the loop analysis result that η affects both lyso-lytic and latent loops, but not the lytic loops. With low latency probability, new infections only grow via lytic loop (unless when T is small enough). As p grows, more new infections grow via lyso-lytic and latent loops.

It is also worth noting that according to our parameter choice with $d' = 0.004, b'_0 = 0.0045$, the vertical fitness$P_3 = \frac{b'_0}{d'+\eta} > 1$ when η is choosen less than 0.0005. Combined with the results from section 4.3.2.1 above that $R_{\text{eff}} > P_3$, $R_{\text{eff}} > 1$ with $\eta < 0.0005$ and causes exponential growth. This result could also be confirmed in Figure 3.3.

Next we analyze the sensitivity of p and η with fixed a fixed latent probability T around the point of $p = 10^{-6}, \eta = 10^{-3}$. The result is shown in Figure 3.4. Here we vary p between $10^{-7} \sim 10^{-5}$ and η between $10^{-5} \sim 10^{-2}$, both are log stepped. It is shown that when T cell density is low $(10^4, 10^5)$ and susceptible cells are lack in the environment,

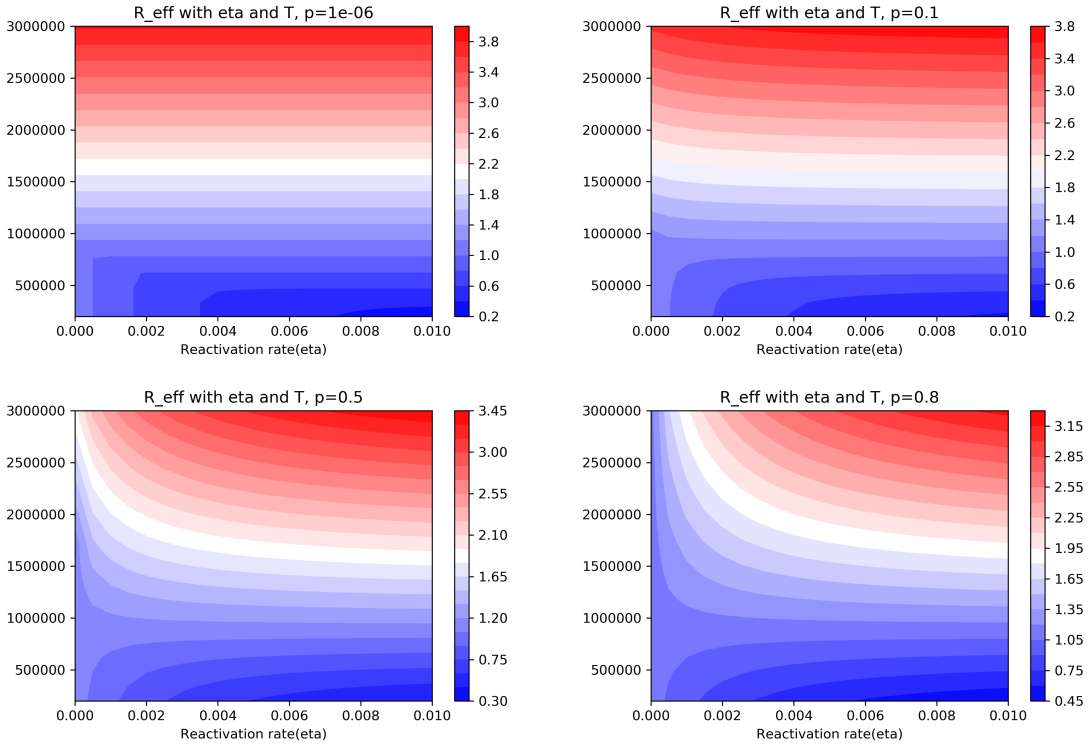

Figure 3.3: Contour for sensitivity analysis of R_{eff} about η and T with fixed $p = 10^{-6}, 0.1, 0.5, 0.8$, colorbar attached. Each contour is drawn with 20 color steps. Horizontal label: η, sampled between $0 \sim 0.01$. Vertical label: T, sampled between $0.1 \sim 1.5 \times T^{\star}$. Both are linearly stepped with 20 steps.

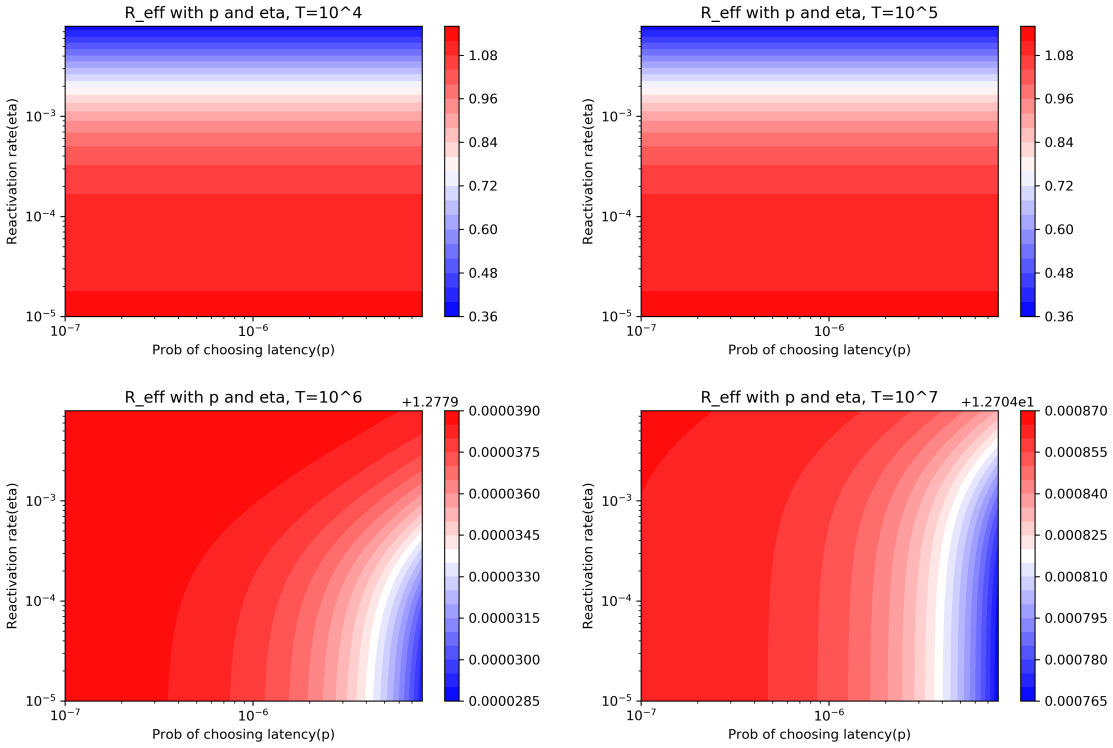

Figure 3.4: Contour for sensitivity analysis of R_{eff} about p and η with fixed $T = 10^4, 10^5, 10^6, 10^7$, colorbar attached. Each contour is drawn with 20 color steps. Horizontal label: p, sampled between $10^{-7} \sim 10^{-5}$ (log transformed in scale). Vertical label: η, sampled between $10^{-5} \sim 10^{-2}$ (log transformed in scale). Both are log stepped with 10 steps.

R_{eff} is negatively related to η and has nearly no relationship with p, η is the dominant parameter; while when T cell density is high $(10^6, 10^7)$ and susceptible cells are abundant, R_{eff} is positively related to η and negatively related to p, p is the dominant parameter.

To quantitatively verify this intuition, we calculated the partial derivative of R_{eff} with η and p. We found that $\frac{\partial R_{\text{eff}}}{\partial \eta}$ is negatively related to $\frac{\partial R_{\text{eff}}}{\partial p}$:

$$\frac{\partial R_{\text{eff}}}{\partial \eta} = -\frac{1}{d' + \eta}\left(p\frac{\partial R_{\text{eff}}}{\partial p} + P_3\left(\frac{P_1 + P_2 + P_3 - 2\frac{P_1}{1-p}}{\sqrt{(P_1 + P_2 + P_3)^2 - 4P_1P_3}} + 1\right)\right) \tag{3.11}$$

We also calculated the numerical derivatives with our parameters.Table 3.2 shows the result of derivatives around the point of $p = 10^{-6}, \eta = 10^{-3}$. The result confirms our hypothesis. It corresponds to our loop analysis result that η affects the lyso-lytic loop and

Table 3.2: Sensitivity analysis of R_{eff} about p and η around the point of $p = 10^{-6}, \eta = 10^{-3}$

p	η	T	$\frac{\partial R_{\text{eff}}}{\partial p}\Big\vert_{\eta=10^{-3},p=10^{-6}}$	$\frac{\partial R_{\text{eff}}}{\partial \eta}\Big\vert_{\eta=10^{-3},p=10^{-6}}$
10^{-6}	10^{-3}	10^{4}	0.0052	-360
10^{-6}	10^{-3}	10^{5}	0.060	-360
10^{-6}	10^{-3}	10^{6}	-0.83	5.60e-04
10^{-6}	10^{-3}	10^{7}	-20	4.29e-03

latent loop (vertical transmission), while p affects the lysis and lyso-lytic loop (horizontal transmission). When susceptible cells are abundant, the horizontal transmission is dominant; when susceptible cells are deficient, vertical transmission is dominant.

Fraction of latent cell at steady state

The goal in this part is to learn about how the adaptive strategy affects the dynamics. We are also interested in how does virus change its strategy to fit the environment. Here we use both simulation and computation methods to analyze the fraction of latent cells at steady state given different p and η. Figure 3.5 shows the fraction of L in all cells ($\frac{L}{T+E+I+L}$, left) and in infected cells ($\frac{L}{E+I+L}$, right) at steady state. It is clear that the fraction is positively related to p, negatively related with η. p is the dominant parameter in L fraction compared to η.

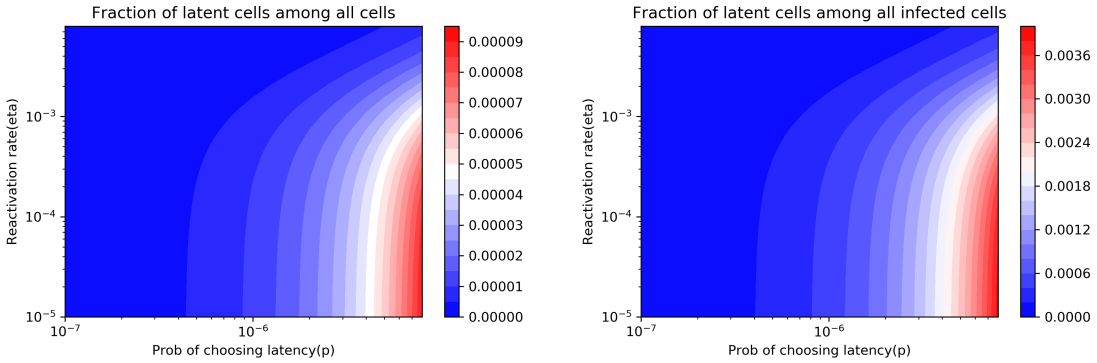

Figure 3.5: Contour for fraction of L in all cells (left) and infected cells (left) about p and η , colorbar attached. Each contour is drawn with 20 color steps. Horizontal label: p, sampled between $10^{-7} \sim 10^{-5}$ (log transformed in scale). Vertical label: η, sampled between $10^{-5} \sim 10^{-2}$ (log transformed in scale). Both are log stepped with 10 steps.

Actually we could solve the steady state by calculation:

$$\begin{aligned}
T^\star &= \frac{\frac{m}{\beta}(\mu+d)}{\frac{k}{a}\frac{\eta+\left(d'+b_0'\right)(1-p)\mu}{\left(\eta+d'-b_0'\right)}-\mu-d} \\
V^\star &= \frac{\lambda}{\beta T^\star}+\frac{b_0-d}{\beta} \\
E^\star &= \frac{\lambda}{\mu+d}+\frac{b_0-d}{\mu+d}T^\star \\
I^\star &= \left(\frac{\eta+\left(d'+b_0'\right)(1-p)}{a\left(\eta+d'-b_0'\right)}\mu\right)E^\star \\
L^\star &= \left(\frac{p\mu}{\eta+d'-b'}\right)E^\star
\end{aligned} \tag{3.12}$$

Our calculation shows that, only L is proportional to p among all states. Therefore, latent cell only takes a small proportion in the system. Since the infected states subsystem is a linear system when T is fixed, all the infected states $E^\star, I^\star, L^\star, V^\star$ are proportional to each other at steady state. Hence, the fraction of L in infected cells is a fixed value:

$$\frac{L^\star}{L^\star+I^\star+E^\star}=\frac{ap\mu}{a\left(p\mu+\eta+d'-b_0'\right)+\mu\left(\eta+\left(d'+b_0'\right)(1-p)\right)} \tag{3.13}$$

Table 3.3: Cell density after simulation for 5000 days. Infected cells choose latency with adaptive strategy.

Lower Bound of p	Upper Bound of p	T density	E density	I density	L density
10^{-6}	10^{-3}	781750.31	11943.75	5976.83	10926.41
10^{-7}	10^{-3}	782334.19	11937.91	5969.45	1091.57
10^{-8}	10^{-3}	781750.32	11943.75	5976.83	10926.29
10^{-6}	10^{-4}	782334.15	11937.91	5969.45	1091.69
10^{-7}	10^{-4}	782334.18	11937.91	5969.45	1091.58
10^{-8}	10^{-4}	782334.19	11937.91	5969.45	1091.57
10^{-6}	10^{-5}	782392.53	11937.33	5968.71	109.25
10^{-7}	10^{-5}	782392.54	11937.33	5968.71	109.15
10^{-8}	10^{-5}	782392.54	11937.33	5968.71	109.15

3.3.3 Fitness analysis with adaptive latent probability

Latent cell density and R_{eff} are both more sensitive to the upper bound of adaptive latent probability

We simulate with the adaptive strategy and investigates on how the range of adaptive latent probability p affects the dynamics of the system and fitness. Figure 3.6 shows the simulation of system dynamics with adaptive p between $[10^{-6}, 10^{-3}]$, $[10^{-6}, 10^{-4}]$, $[10^{-7}, 10^{-3}]$, $[10^{-7}, 10^{-4}]$. For each simulation, p is varied in the region with 20 log steps and returns the value that maximize R_{eff} given current environment parameters. Consider the L density dynamics, the two dynamics with a same upper bound is closer than the two dynamics with the same lower bound.

To quantitatively verify our hypothesis, we simulated the dynamics with different combinations of p range and recorded the cell density at equilibrium. Table 3.3 shows the cell density after 5000 days of simulation, with the lower bound of p chosen among 10^{-6}, 10^{-7}, 10^{-8}, and upper bound of p among 10^{-3}, 10^{-4}, 10^{-5}. The result confirms our statement that the dynamics after long time is not dependent on the lower bound of p, and the latent cell density is nearly proportional to the largest possible latent probability.

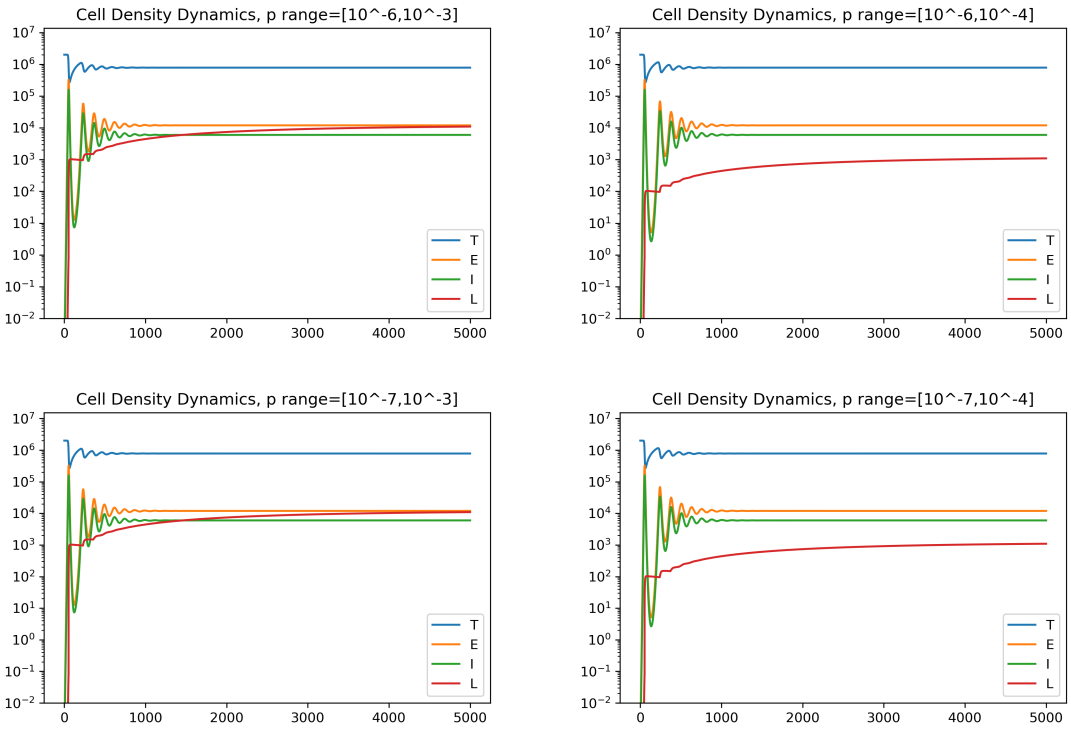

Figure 3.6: Simulation on cell density dynamics with time for 5000 days, $\eta = 10^{-3}$. Infected cells choose latency with adaptive strategy, p varies between the range of $[10^{-6}, 10^{-3}]$, $[10^{-6}, 10^{-4}]$, $[10^{-7}, 10^{-3}]$,$[10^{-7}, 10^{-4}]$. Horizontal label: Time (/day). Vertical label: Cell density (Log transformed).

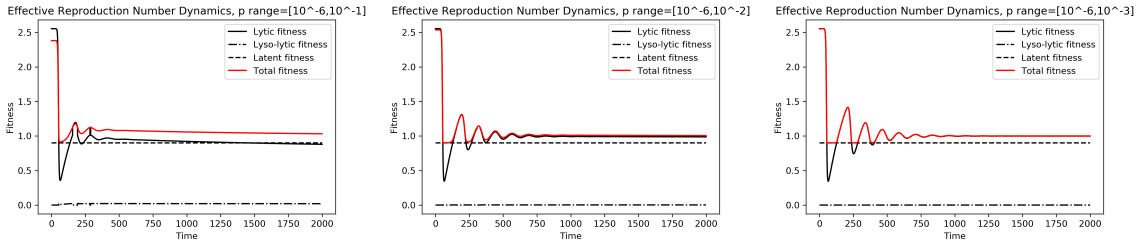

Figure 3.7: Dynamics of regenrated effective reproduction number with simulated cell and virion densities and choice of p in range. Red line: Total R_{eff}. Black line: Lytic loop fitness (P_1). Black dot dash line: Lyso-lytic loop fitness (P_2). Black dash line: Latent loop fitness (P_3). Infected cells choose latency with adaptive strategy between the range of $[10^{-6}, 10^{-1}]$ (left), $[10^{-6}, 10^{-2}]$ (middle), and $[10^{-6}, 10^{-3}]$ (right). Horizontal label: Time (/day). Vertical label: Fitness.

Similar to the constant strategy simulation, we regenerate the fitness dynamics with the simulation result. However, this time, apart from directly calculating with simulated T values, we need to regenerate the choice of p first and then recover R_{eff}. Figure 3.7 shows the regenerated R_{eff} dynamics with time. By changing the upper bound of p range, the dynamics is also largely altered.

All or none: The optimized latent probability is either the largest or smallest possible p, depending on the comparison between horizontal and vertical fitness

To understand when will the virus' choice generate maximized fitness, we need to find the p that maximize R_{eff} and calculate $\frac{dR_{\text{eff}}}{dp}$. Surprisingly we find that $\frac{dR_{\text{eff}}}{dp} > 0$ when $R_{0,ver} > R_{0,hor}$ and $\frac{dR_{\text{eff}}}{dp} < 0$ when $R_{0,ver} < R_{0,hor}$. In other words, R_{eff} grows or decays with respect to p depends on the horizontal fitness ($R_{0,hor}$) and the vertical fitness ($R_{0,ver}$).

Here $R_{0,hor}$ is the fitness of "purely" lysis transmission ($p = 1, \eta = 0$); $R_{0,ver}$ is the fitness of "purely" latent transmission ($p = 0, \eta = 0$). The interesting thing here is though the system is complex and connected, virus disregard the reactivation reaction for its' reference

of selecting strategy.

$$\begin{aligned} &\frac{dR_{\text{eff}}}{dp} * (R_{0,ver} - R_{0,hor}) > 0 \\ &R_{0,ver} = \frac{b_0'}{d'} \\ &R_{0,hor} = \left(\frac{\mu}{d+\mu}\right)\left(\frac{k}{a}\right)\left(\frac{\beta T}{\beta T + m}\right) \end{aligned} \tag{3.14}$$

Since both $R_{0,hor}$ and $R_{0,ver}$ are not dependent on p, R_{eff} is monotonically related to p. Therefore, the p value that maximizes R_{eff} is either the upper bound or the lower bound of the possible region. See Appendix D for calculation in detail.

We also used simulation results to verify this confirm this result. Figure 3.8 shows simulation results for nine different p adaptive ranges. The blue line is division between $R_{0,hor}$ and $R_{0,ver}$. The red line is the optimized p choice at each time point in our simulation. The result confirms our conclusion that the optimized choice of p is switching between the upper bound and lower bound of p range. The switching point depends on the comparison between $R_{0,hor}$ and $R_{0,ver}$.

The figure also shows that after long-term infection, the choice of p gets stable at the maximal value. This is because the horizontal fitness $R_{0,hor}$ is dependent on the environment and converges to 1 at steady state. The vertical fitness, however, is not dependent on the environment and is always greater than 1, since the growth rate of latent cell is greater than decay rate ($b_0' > d'$). Hence, after long-term infection, $R_{0,ver} > R_{0,hor}$ and $\frac{dR_{\text{eff}}}{dp} > 0$. This explains why the cell density dynamics and fitness dynamics are both more dependent on the upper bound of p range.

3.3.4 Comparison analysis of fitness with constant and adaptive latent probability

To get more understanding in each strategies evolutionary benefits, we compare the dynamics of constant strategy and adaptive strategy. First we compare the system dynamics

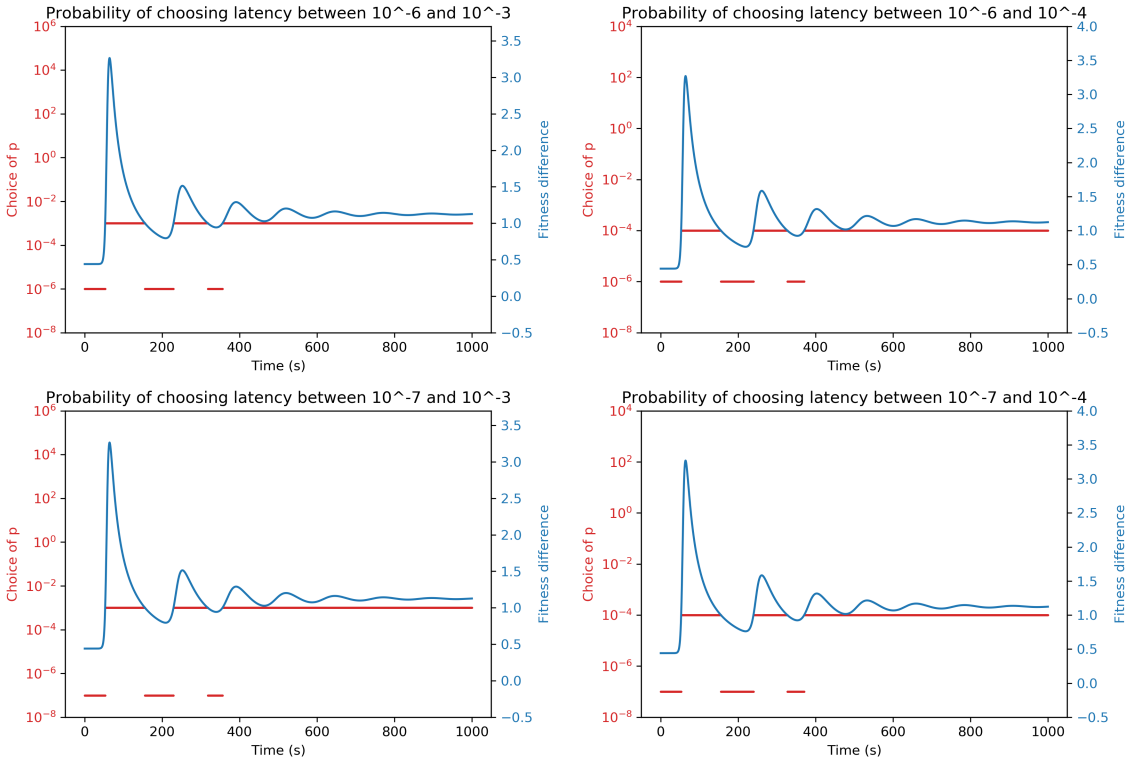

Figure 3.8: Dynamics of optimized p and division between $R_{0,hor}$ and $R_{0,ver}$. Blue line: $\frac{R_{0,ver}}{R_{0,hor}}$. Red line: optimized choice of p. Horizontal label: Time (/day). Vertical label left: Latent possibility p.

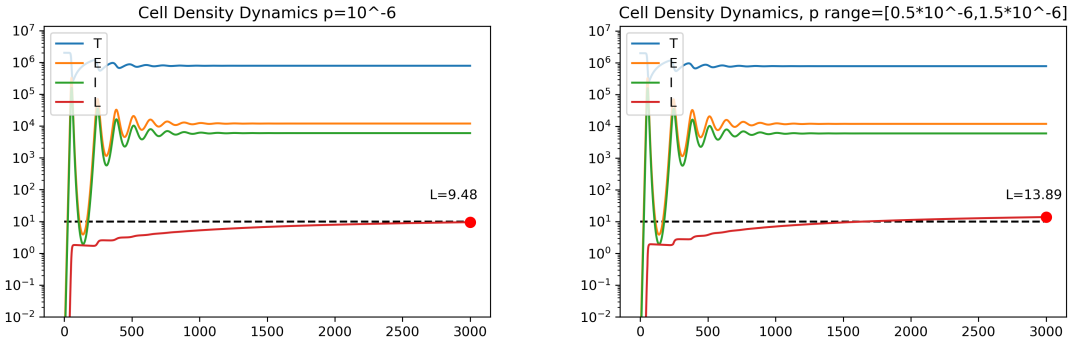

Figure 3.9: Simulation on cell density dynamics with time for 3000 days, $\eta = 10^{-3}$. Infected cells choose latency with constant strategy, $p = 10^{-6}$ (left), and with adaptive strategy, p varies between the range of $[0.5 \times 10^{-6}, 1.5 \times 10^{-6}]$. Black dashed line: horizontal line (10^1) for reference to compare values of L in left and right panels. Horizontal label: Time (/day). Vertical label: Cell density (Log transformed).

based on the different strategies. Figure 3.9 shows the simulated dynamics with a constant $p = 10^{-6}$ and p varies between $[0.5 \times 10^{-6}, 1.5 \times 10^{-6}]$ with all other parameters the same. We choose the mean value of the adaptive range the same with the constant value. At time point 3000 (days), we measured the L density for both strategies. Compared to the constant strategy (9.48), adaptive strategy shows a higher density of L at the same time point (13.89). The dashed black lines in both figures are horizontal line $y = 10^1$ that assists comparison.

Next, we compare the dynamics of fitness based on the different strategies. Figure 3.9 shows the simulated dynamics with a constant $p = 10^{-6}$ (left), $p = 10^{-1}$ (right) and p varies between $[10^{-6}, 10^{-1}]$ (middle) with all other parameters the same. The R_{eff} dynamics between the adaptive strategy and constant strategy with $p = 0.1$ (upper bound of the adaptive p range) is similar (t-test p-value = 0.6953), however is totally different from constant strategy with $p = 10^{-6}$ (t-test p-value = 10^{-97}). We can conclude that R_{eff} is majorly dependent on the upper bound of p range. We could estimate the R_{eff} dynamics of adaptive strategy by the constant strategy with the upper bound of p range.

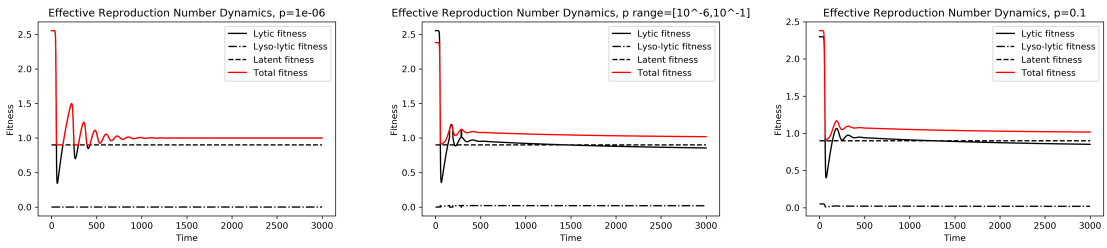

Figure 3.10: Dynamics of regenrated effective reproduction number with simulated cell and virion densities and choice of p in range. Red line: Total R_{eff}. Black line: Lytic loop fitness (P_1). Black dot dash line: Lyso-lytic loop fitness (P_2). Black dash line: Latent loop fitness (P_3). Infected cells choose latency with constant strategy, $p = 10^{-6}$ (left), $p = 10^{-1}$ (right) and with adaptive strategy between the range of $[10^{-6}, 10^{-1}]$(middle). Horizontal label: Time (/day). Vertical label: Fitness.

CHAPTER 4

DISCUSSION

The presence of latent cells in the with-in host system is like a reservoir. When the concentration of susceptible cells is too low to produce new infections, the infected cells can gain higher fitness by entering the latent state. With the reactivation from latent state to acute state, latently infected cells could wait until the rebound of susceptible cell density and produce new virions when susceptible cells become more abundant. The reactivation event also builds a connection between the lytic loop and the latent loop. Contrary to intuition, our result shows that the total reproduction number is the average reproduction number of one generation and two generation loops. Moreover, the reproduction number of one generation loops is simply the sum of all three loops' reproduction numbers, but not the averaged value. Therefore, the total fitness is higher than the fitness of any of these three single loops. This conclusion indicates that infected cells contribute simultaneously to the total infection by entering different proliferation paths. Even when an environment is not conducive to any single viral pathway's growth, the multiple paths could combine and maintain an equilibrium at low density instead of dying out.

Next, we evaluated a hypothetical scenario to explore the relationship between conditions and the potentially adaptive strategy of latent infections. All results showed high sensitivity on the upper bound of the latent probability range. There is not much difference in comparing the dynamics of adaptive strategy with the dynamics of constant strategy of the maximal latent probability only. Therefore, we could conclude that the dynamics of adaptive strategy is dependent on the maximal latent probability instead of the mean latent probability. It implies that in most of the scenarios, vertical proliferation is preferred than horizontal growth based on our parameter choice.

We also found that the optimized choice of p switches between the maximal and mini-

mal of the possible range. In spite of the system connectivity, infected cells only refer to the fitness in purely single loops in non-connected situations when making strategy switches. Since the strategy switch is only determined by the environment and is not related to latent probability, all infected cells adopt the same strategy and lead to radical change in the environment. As feedback, infected cells need to re-adjust their strategy, results in the switch back and forth.

We also used both calculation and simulation methods to estimate the fraction of latent cells at steady state in the system. Our result shows that the fraction is close to the proportional of latent probability p. Given the low value of the latent probability around 10^{-6}, we would expect small numbers of latent cells. Therefore, taking ART drugs and eliminating acutely infected cells in this model would suppress the infected cell density and viral load to an undetectable level.

In addition, this work suggests potential evolutionary benefits if HIV were to respond to the state of the environment. This idea seems ideal for experimental tests. For example, how does cellular fate, i.e., active infections or latency, depend on external cell density? If there is a dependency, does fate depend on current and/or prior states? Any such evidence would also raise questions on the molecular and cellular factors driving such changes. Recent research has found that HIV latency is mediated by epigenetic silencing and interruption of Tat expression driven regulatory feedback[25, 26, 27, 28]. There have been some studies on HIV viral structural proteins' ability of sensing change in the environment (gag, env, pol proteins). It is shown that gag protein can sense the cholesterol and acyl chain environment in model membranes[29]. However, there is no comprehensive protein pathway studies on the HIV sensory system so far. The mechanism by which susceptible cells estimate HIV density in the environment is largely unresolved.

Setting new metrics for HIV to change strategies is another direction of exploration. Our current fitness measurements are based on the strategy that maximize effective production number (i.e. cause as many infections as possible in the next generation). However,

evolution acts on the entirety of the viral replication cycle, both inside and outside hosts. We might decide to evaluate other metrics: for example, to maximize the number of new generations of new viruses or the number of new latent infected cells.

There are still many aspects that can improve this work. One of the main ideas is to improve the model, especially to add the immune response to the model for analysis. In addition, apart from the natural linear decay of the infected cells, HIV kills the acutely infected cells actively by inducing apoptosis and pyroptosis[2, 3]. Taking more players and reactions into account in the system would exponentially increase the complexity of analysis work.

There are some potential experiments that can be implemented to combine with our results. Many in vitro systems have been developed to study HIV latency and reactivation[30]. These systems present an opportunity to test the model here. For example, consider the case of extracting HIV in vitro and exposing it to different concentrations of susceptible cells. After a period of infection, it should be possible to determine the fraction of infected cells that enter latency. Our model predicts that the latency fraction should decrease with infected cell densities. Next, after the infection reaches an equilibrium level at a certain cell concentration, it is possible to change the concentration of susceptible cells and measure the reactivation from latency as well as the proliferation of latent cells. We predict that re-activation rates can also depend sharply on availability of uninfected cells. These initial in vitro experiments may help inform similar experiments within HIV strains from animal models and/or humans.

In summary, this thesis helps to advance a long-term goal to build a combined within-host and between-hosts modeling framework for the evolution of HIV latency. The within-host fitness of virus influences the outcome of contact between a susceptible host and an infected host[31, 32]. Therefore, whether transmission events occur is dependent on the within-host fitness. Our results in this paper provide some insights for analysis on more complex models, including those that bridge the gap between short-term optimization (con-

sidered here) and long-term evolutionary dynamics both within and between hosts.

Appendices

APPENDIX A

NEXT GENERATION MATRIX METHOD

The Jacobian matrix provides the linearization around the pathogen free equilibrium, $[T^\star, 0, 0, 0, 0]$. Here we decompose the Jacobian matrix into the transition matrix:

$$T = \begin{bmatrix} -d-\mu & 0 & 0 & 0 \\ \mu\,(1-p) & -a & \eta & 0 \\ \mu p & 0 & -d'-\eta & 0 \\ 0 & k & 0 & -\beta T^\star - m \end{bmatrix} \tag{A.1}$$

Transmission matrix:

$$\Sigma = \begin{bmatrix} 0 & 0 & 0 & \beta T^\star \\ 0 & 0 & 0 & 0 \\ 0 & 0 & b_0' & 0 \\ 0 & 0 & 0 & 0 \end{bmatrix} \tag{A.2}$$

Hence, the NGM matrix could be calculated as:

$$K_L = -T\Sigma^{-1} = \begin{bmatrix} (\frac{\mu}{d+\mu})(\frac{k}{a})(\frac{\beta T^\star}{\beta T^\star+m})(\frac{d'(1-p)+\eta}{d'+\eta}) & (\frac{\beta T^\star}{\beta T^\star+m})(\frac{k}{a}) & (\frac{\beta T^\star}{\beta T^\star+m})(\frac{k}{a})(\frac{\eta}{d'+\eta}) & \frac{\beta T^\star}{\beta T^\star+m} \\ 0 & 0 & 0 & 0 \\ (\frac{b_0'}{d'+\eta})(\frac{\mu p}{d+\mu}) & 0 & \frac{b_0'}{d'+\eta} & 0 \\ 0 & 0 & 0 & 0 \end{bmatrix} \tag{A.3}$$

It is clear that the second row and fourth row of NGM are all zeros. It corresponds to our model that only two states, E and L, can produce new infected individuals.

APPENDIX B

TOTAL FITNESS CALCULATION

Here we calculate that with a constant latent probability p, provided with the condition that fitness in all paths are positive, the total fitness R_{eff} is greater than the lysis loop fitness P_1.

$$\begin{aligned}
&R_0 = \frac{(P_1+P_2+P_3)+\sqrt{(P_1+P_2+P_3)^2-4P_1P_3}}{2} > P_1 \\
&\Leftrightarrow (P_1+P_2+P_3)+\sqrt{(P_1+P_2+P_3)^2-4P_1P_3} > 2P_1 \\
&\Leftrightarrow \sqrt{(P_1+P_2+P_3)^2-4P_1P_3} > P_1-P_2-P_3 \\
&\Leftarrow (P_1+P_2+P_3)^2-4P_1P_3 > (P_1-P_2-P_3)^2 \\
&\Leftrightarrow \Sigma P_i^2+2P_1P_2+2P_2P_3-2P_1P_3 > \Sigma P_i^2-2P_1P_2+2P_2P_3-2P_1P_3 \\
&\Leftrightarrow P_1P_2 > 0
\end{aligned} \tag{B.1}$$

Since $P_1 > 0, P_2 > 0$, the inequality is satisfied. In the same way we can calculate that $R_{eff} > P_3$.

On the other hand, we could calculate that $R_{eff} > P_2$:

$$\begin{aligned}
&R_0 = \frac{(P_1+P_2+P_3)+\sqrt{(P_1+P_2+P_3)^2-4P_1P_3}}{2} > P_2 \\
&\Leftrightarrow (P_1+P_2+P_3)+\sqrt{(P_1+P_2+P_3)^2-4P_1P_3} > 2P_2 \\
&\Leftrightarrow \sqrt{(P_1+P_2+P_3)^2-4P_1P_3} > P_2-P_1-P_3
\end{aligned} \tag{B.2}$$

Since p is small (around 10^{-6}), P_2 is smaller than $(P_1 + P_3)$. The left side of the inequality is positive and right side of the inequality is negative. Hence, the inequality is already satisfied.

APPENDIX C

STEADY STATE CALCULATION

We mathematically calculate the steady state with a constant latent probability p. In our calculation, we show that $E^\star, I^\star, L^\star, V^\star$ are proportional to each other.

$$
\begin{aligned}
\dot{L} = 0 \Rightarrow L^\star &= (\frac{p\mu}{\eta + d' - b'})E^\star \\
\dot{I} = 0 \Rightarrow I^\star &= (\frac{\eta + (d' + b'_0)(1-p)}{a(\eta + d' - b'_0)}\mu)E^\star \\
\dot{E} + \dot{V} = 0 \Rightarrow V^\star &= (\frac{\frac{k}{a}\frac{\eta+(d'+b'_0)(1-p)\mu}{(\eta+d'-b'_0)} - \mu - d}{m})E^\star \\
\dot{E} = 0 \Rightarrow T^\star &= \frac{(\mu + d)E^\star}{\beta V^\star} \\
\Rightarrow T^\star &= \frac{\frac{m}{\beta}(\mu + d)}{\frac{k}{a}\frac{\eta+(d'+b'_0)(1-p)\mu}{(\eta+d'-b'_0)} - \mu - d} \\
V^\star &= \frac{\lambda + b_0 T^\star - dT^\star}{\beta T^\star} = \frac{\lambda}{\beta T^\star} + \frac{b_0 - d}{\beta} \\
E^\star &= \frac{\lambda}{\mu + d} + \frac{b_0 - d}{\mu + d} T^\star
\end{aligned}
\tag{C.1}
$$

APPENDIX D

R_{EFF} IS MONOTONIC WITH P

To prove that R_{eff} monotonically increases or decreases with p, we calculate $\frac{dR_{eff}}{dp}$. Here we calculate that $\frac{dR_{eff}}{dp} > 0 \Leftrightarrow R_{0,ver} > R_{0,hor}$.

First we set the variables as:

$$\begin{aligned} X &= (\frac{k}{a})(\frac{\beta T^{\star}}{\beta T^{\star} + m}) \\ Y &= \frac{b_0'}{d' + \eta} \\ F &= (X\mu\left(d'\left(p-1\right) - \eta\right) + Y\left(d+\mu\right)\left(d'+\eta\right)) \end{aligned} \tag{D.1}$$

With the variable substitution:

$$\frac{dR_{eff}}{dp} = \frac{X\mu\left(2Y\eta\left(d+\mu\right)\left(d'+\eta\right) - d'\sqrt{4XY\eta\mu p\left(d+\mu\right)\left(d'+\eta\right) + F^2} + d'F\right)}{\sqrt{4XY\eta\mu p\left(d+\mu\right)\left(d'+\eta\right) + F^2}\left(d+\mu\right)\left(d'+\eta\right)} \tag{D.2}$$

$$
\begin{aligned}
\frac{dR_{eff}}{dp} > 0 &\Leftrightarrow 2Y\eta\left(d+\mu\right)\left(d'+\eta\right) - d'\sqrt{4XY\eta\mu p\left(d+\mu\right)\left(d'+\eta\right)+F^2} + d'F > 0 \\
&\Leftrightarrow 2Y\eta\left(d+\mu\right)\left(d'+\eta\right) + d'F > d'\sqrt{4XY\eta\mu p\left(d+\mu\right)\left(d'+\eta\right)+F^2} \\
&\Leftrightarrow \left(2Y\eta\left(d+\mu\right)\left(d'+\eta\right) + d'F\right)^2 > (d')^2(4XY\eta\mu p\left(d+\mu\right)\left(d'+\eta\right)+F^2) \\
&\Leftrightarrow 4Y^2\eta^2\left(d+\mu\right)^2\left(d'+\eta\right)^2 + 4Y\eta\left(d+\mu\right)\left(d'+\eta\right)d'F > (d')^2 4XY\eta\mu p\left(d+\mu\right)\left(d'+\eta\right) \\
&\Leftrightarrow Y\eta\left(d+\mu\right)\left(d'+\eta\right) + d'F > (d')^2 X\mu p \\
&\Leftrightarrow Y\eta\left(d+\mu\right)\left(d'+\eta\right) + d'\left(X\mu\left(d'\left(p-1\right)-\eta\right) + Y\left(d+\mu\right)\left(d'+\eta\right)\right) > (d')^2 X\mu p \\
&\Leftrightarrow Y\left(d+\mu\right)\left(d'+\eta\right)^2 > d'X\mu(d'(1-p)+\eta) + (d')^2 X\mu p \\
&\Leftrightarrow Y\left(d+\mu\right)\left(d'+\eta\right)^2 > d'X\mu\left(d'+\eta\right) \\
&\Leftrightarrow \frac{Y}{d'}\left(d'+\eta\right) > \frac{X\mu}{(d+\mu)} \\
&\Leftrightarrow \frac{b'_0}{d'} > (\frac{\mu}{d+\mu})(\frac{k}{a})(\frac{\beta T^\star}{\beta T^\star + m})
\end{aligned}
\tag{D.3}
$$

APPENDIX E

MAIN CODE

All source code based on Python 3.7.0.

```
import numpy as np
import matplotlib.pyplot as plt
from scipy import integrate
from scipy import optimize
from scipy import stats
from numpy import linalg
import sympy as sym
import math
import pandas as pd
import ipynb
import matplotlib.ticker as ticker

pars = {}
pars['lambda'] = 10**4
pars['d'] = 0.01
pars['d1'] = 0.004
pars['a'] = 1
pars['m'] = 23
pars['beta'] = 1.5*10**-8
pars['k'] = 2000
pars['b0'] = 0.005    #smaller than d
pars['b1'] = 0.0045
pars['mu'] = 0.5
pars['p'] = 0.01
pars['eta'] = 0.001
T0 = pars['lambda']/(pars['d']-pars['b0'])

# Calculate R0 with the NGM matrix result
# Params: T(Density), p(prob choosing latency), eta(reactivation rate)
def R0(T,p,eta):
    A = pars['mu']/(pars['d']+pars['mu'])*pars['k']/pars['a']*pars['beta
        ']*T/(pars['beta']*T+pars['m'])*(pars['d1']*(1-p)+eta)/(pars['d1
        ']+eta)
    B = pars['beta']*T/(pars['beta']*T+pars['m'])*pars['k']/pars['a']*
        eta/(pars['d1']+eta)
    C = pars['b1']/(pars['d1']+eta) * pars['mu']*p/(pars['d']+pars['mu
        '])*np.ones_like(T)
    D = pars['b1']/(pars['d1']+eta)*np.ones_like(T)
    R0 = ((A+D)+np.sqrt((A-D)**2+4*B*C))/2
    return R0

# Calculate the p(prob) that maximize the effective reproduction number
# Params: T, upper and lower bound of log(p), number of steps
```

```
# Choose a log step
# Prefered bounds: -7 and -5
def maxR0(T, step, p_lower, p_upper):
    R0_space = []
    p_space = 10**np.linspace(p_lower,p_upper,step+1)
    if(pars['eta'] != 0):
        for p in p_space:
            R0_space.append(R0(T,p,pars['eta']))
        tmp = p_space[np.where(R0_space == np.max(R0_space))]
        if(len(tmp) != 1):
            p_selected = np.random.choice(tmp)
            print(tmp)
        else:
            p_selected = tmp[0]
    else:
        R0_hor = pars['mu']/(pars['d']+pars['mu'])*pars['k']/pars['a']*
           pars['beta']*T/(pars['beta']*T+pars['m'])*(1-pars['p'])
        R0_ver = pars['b1']/pars['d1']
        if(R0_hor > R0_ver):
            p_selected = p_space[0]
        else:
            p_selected = p_space[-1]
    return(p_selected)

# Dynamics with a constant p value
# Params: Original states, time, pars
def dynamics_const(y, t, pars):
    T = y[0]
    E = y[1]
    I = y[2]
    L = y[3]
    V = y[4]
    N = T+E+L+I
    dTdt = pars['lambda'] + pars['b0']*T - pars['d']*T - pars['beta']*V*
       T
    dEdt = pars['beta']*V*T - pars['mu']*E - pars['d']*E
    dIdt = (1-pars['p'])*pars['mu']*E - pars['a']*I + pars['eta']*L
    dLdt = pars['p']*pars['mu']*E + pars['b1']*L - pars['d1']*L - pars['
       eta']*L
    dVdt = pars['k']*I - pars['m']*V - pars['beta']*V*T
    dyn = [dTdt, dEdt, dIdt, dLdt, dVdt]
    return(dyn)

# Dynamics with an adaptive p value
# Choose p with maxR0 in each step
# Params: Original states, time, pars, upper and lower bound of log(p)
def dynamics_feedback(y, t, pars, p_lower, p_upper):
    T = y[0]
    E = y[1]
    I = y[2]
    L = y[3]
    V = y[4]
    N = T+E+L+I
    pars['p'] = maxR0(T,10, p_lower, p_upper)
```

```
dTdt = pars['lambda'] + pars['b0']*T - pars['d']*T - pars['beta']*V*
    T
dEdt = pars['beta']*V*T - pars['mu']*E - pars['d']*E
dIdt = (1-pars['p'])*pars['mu']*E - pars['a']*I + pars['eta']*L
dLdt = pars['p']*pars['mu']*E + pars['b1']*L - pars['d1']*L - pars['
    eta']*L
dVdt = pars['k']*I - pars['m']*V - pars['beta']*V*T
dyn = [dTdt, dEdt, dIdt, dLdt, dVdt]
return(dyn)
```

REFERENCES

[1] M. A. Nowak and R. M. May, *Virus dynamics: mathematical principles of immunology and virology*. Oxford ; New York: Oxford University Press, 2000, ISBN: 9780198504177 9780198504184.

[2] N. W. Cummins and A. D. Badley, "Making sense of how HIV kills infected CD4 T cells: Implications for HIV cure," *Molecular and Cellular Therapies*, vol. 2, no. 1, p. 20, 2014.

[3] T. H. Finkel and N. K. Banda, "Indirect mechanisms of HIV pathogenesis: How does HIV kill T cells?" *Current Opinion in Immunology*, vol. 6, no. 4, pp. 605–615, Aug. 1994.

[4] D. C. Chan and P. S. Kim, "HIV Entry and Its Inhibition," *Cell*, vol. 93, no. 5, pp. 681–684, May 1998.

[5] R. Wyatt and J. Sodroski, "The HIV-1 Envelope Glycoproteins: Fusogens, Antigens, and Immunogens," *Science*, vol. 280, no. 5371, pp. 1884–1888, Jun. 1998.

[6] R. F. Siliciano and W. C. Greene, "HIV Latency," *Cold Spring Harbor Perspectives in Medicine*, vol. 1, no. 1, a007096, Sep. 2011.

[7] P. A. Volberding and S. G. Deeks, "Antiretroviral therapy and management of HIV infection," *The Lancet*, vol. 376, no. 9734, pp. 49–62, Jul. 2010.

[8] A. M. Crooks, R. Bateson, A. B. Cope, N. P. Dahl, M. K. Griggs, J. D. Kuruc, C. L. Gay, J. J. Eron, D. M. Margolis, R. J. Bosch, and N. M. Archin, "Precise Quantitation of the Latent HIV-1 Reservoir: Implications for Eradication Strategies," *Journal of Infectious Diseases*, vol. 212, no. 9, pp. 1361–1365, Nov. 2015.

[9] R. Lorenzo-Redondo, H. R. Fryer, T. Bedford, E.-Y. Kim, J. Archer, S. L. Kosakovsky Pond, Y.-S. Chung, S. Penugonda, J. G. Chipman, C. V. Fletcher, T. W. Schacker, M. H. Malim, A. Rambaut, A. T. Haase, A. R. McLean, and S. M. Wolinsky, "Persistent HIV-1 replication maintains the tissue reservoir during therapy," *Nature*, vol. 530, no. 7588, pp. 51–56, Feb. 2016.

[10] D. Finzi, "Identification of a Reservoir for HIV-1 in Patients on Highly Active Antiretroviral Therapy," *Science*, vol. 278, no. 5341, pp. 1295–1300, Nov. 1997.

[11] D. Finzi, J. Blankson, J. D. Siliciano, J. B. Margolick, K. Chadwick, T. Pierson, K. Smith, J. Lisziewicz, F. Lori, C. Flexner, T. C. Quinn, R. E. Chaisson, E. Rosenberg,

B. Walker, S. Gange, J. Gallant, and R. F. Siliciano, "Latent infection of CD4+ T cells provides a mechanism for lifelong persistence of HIV-1, even in patients on effective combination therapy," *Nature Medicine*, vol. 5, no. 5, pp. 512–517, May 1999.

[12] J. D. Siliciano, J. Kajdas, D. Finzi, T. C. Quinn, K. Chadwick, J. B. Margolick, C. Kovacs, S. J. Gange, and R. F. Siliciano, "Long-term follow-up studies confirm the stability of the latent reservoir for HIV-1 in resting CD4+ T cells," *Nature Medicine*, vol. 9, no. 6, pp. 727–728, Jun. 2003.

[13] D. B. Reeves, E. R. Duke, T. A. Wagner, S. E. Palmer, A. M. Spivak, and J. T. Schiffer, "A majority of HIV persistence during antiretroviral therapy is due to infected cell proliferation," *bioRxiv*, Sep. 2018.

[14] A. L. Hill, D. I. S. Rosenbloom, M. A. Nowak, and R. F. Siliciano, "Insight into treatment of HIV infection from viral dynamics models," *Immunological Reviews*, vol. 285, no. 1, pp. 9–25, Sep. 2018.

[15] A. L. Hill, "Modeling HIV persistence and cure studies:" *Current Opinion in HIV and AIDS*, p. 1, Jul. 2018.

[16] J. M. Conway and A. S. Perelson, "Post-treatment control of HIV infection," *Proceedings of the National Academy of Sciences*, vol. 112, no. 17, pp. 5467–5472, Apr. 2015.

[17] S. A. Azoz and D. Coombs, "Stochastic Dynamics of the Latently Infected Cell Reservoir During HIV Infection," *Bulletin of Mathematical Biology*, vol. 81, no. 1, pp. 131–154, Jan. 2019.

[18] N. M. Archin, N. K. Vaidya, J. D. Kuruc, A. L. Liberty, A. Wiegand, M. F. Kearney, M. S. Cohen, J. M. Coffin, R. J. Bosch, C. L. Gay, J. J. Eron, D. M. Margolis, and A. S. Perelson, "Immediate antiviral therapy appears to restrict resting CD4+ cell HIV-1 infection without accelerating the decay of latent infection," *Proceedings of the National Academy of Sciences*, vol. 109, no. 24, pp. 9523–9528, Jun. 2012.

[19] O. Diekmann, J. Heesterbeek, and J. Metz, "On the definition and the computation of the basic reproduction ratio R 0 in models for infectious diseases in heterogeneous populations," *Journal of Mathematical Biology*, vol. 28, no. 4, Jun. 1990.

[20] O. Diekmann, J. A. P. Heesterbeek, and M. G. Roberts, "The construction of next-generation matrices for compartmental epidemic models," *Journal of The Royal Society Interface*, vol. 7, no. 47, pp. 873–885, Jun. 2010.

[21] O. F. Brandenberg, C. Magnus, P. Rusert, H. F. Günthard, R. R. Regoes, and A. Trkola, "Predicting HIV-1 transmission and antibody neutralization efficacy in vivo

from stoichiometric parameters," *PLOS Pathogens*, vol. 13, no. 5, J. Yin, Ed., e1006313, May 2017.

[22] P. van den Driessche, "Reproduction numbers of infectious disease models," *Infectious Disease Modelling*, vol. 2, no. 3, pp. 288–303, Aug. 2017.

[23] G. Li, M. H. Cortez, and J. S. Weitz, "Why be Temperate: On the Fitness Benefits of Lysis vs. Lysogeny," *Preprint*,

[24] R. Levins, "Discussion paper: The qualitative analysis of partially specified systems," *Annals of the New York Academy of Sciences*, vol. 231, no. 1, pp. 123–138, 1974.

[25] D. C. Cary, K. Fujinaga, and B. M. Peterlin, "Molecular mechanisms of HIV latency," *The Journal of Clinical Investigation*, vol. 126, no. 2, pp. 448–454,

[26] S. Hakre, L. Chavez, K. Shirakawa, and E. Verdin, "HIV latency: Experimental systems and molecular models," *FEMS Microbiology Reviews*, vol. 36, no. 3, pp. 706–716, May 2012.

[27] J. Karn, "The molecular biology of HIV latency: Breaking and restoring the Tat-dependent transcriptional circuit," *Current opinion in HIV and AIDS*, vol. 6, no. 1, pp. 4–11, Jan. 2011.

[28] U. Mbonye and J. Karn, "Transcriptional control of HIV latency: Cellular signaling pathways, epigenetics, happenstance and the hope for a cure," *Virology*, vol. 454-455, pp. 328–339, Apr. 2014.

[29] R. A. Dick, S. L. Goh, G. W. Feigenson, and V. M. Vogt, "HIV-1 Gag protein can sense the cholesterol and acyl chain environment in model membranes," *Proceedings of the National Academy of Sciences*, vol. 109, no. 46, pp. 18 761–18 766, Nov. 2012.

[30] J. M. Zerbato, E. Serrao, G. Lenzi, B. Kim, Z. Ambrose, S. C. Watkins, A. N. Engelman, and N. Sluis-Cremer, "Establishment and Reversal of HIV-1 Latency in Naive and Central Memory CD4 $^{+}$ T Cells *In Vitro*," *Journal of Virology*, vol. 90, no. 18, G. Silvestri, Ed., pp. 8059–8073, Sep. 2016.

[31] M. A. Gilchrist and D. Coombs, "Evolution of virulence: Interdependence, constraints, and selection using nested models," *Theoretical Population Biology*, vol. 69, no. 2, pp. 145–153, Mar. 2006.

[32] D. Coombs, M. A. Gilchrist, and C. L. Ball, "Evaluating the importance of within- and between-host selection pressures on the evolution of chronic pathogens," *Theoretical Population Biology*, vol. 72, no. 4, pp. 576–591, Dec. 2007.